Supplementary Note

Tunable Magnetic Confinement Effect in a Magnetic Superlattice of Graphene

Onur Tosun[1], Preetha Sarkar[1], Chang Qian[2], Matthew Gilbert[3], Qian Chen[2], and Nadya Mason[4]

[1]Department of Physics and Materials Research Laboratory, University of Illinois, Urbana, IL, USA; [2]Department of Materials Science and Engineering, University of Illinois Urbana Champaign, IL, USA; [3]Department of Electrical and Computer Engineering, University of Illinois, Urbana, IL, USA; [4]Pritzker School of Molecular Engineering, University of Chicago, Chicago, IL, USA.

Correspondence: Onur Tosun (onurtosunn@gmail.com) or Nadya Mason (nmason1@uchicago.edu)

Supplementary Note 1

The Fe_3O_4 nanoparticles were synthesized following a literature reported method [1]. An iron-oleate complex was first prepared by dissolving 10.8 g iron chloride ($FeCl_3 \cdot 6H_2O$, Aldrich) and 36.5 g of sodium oleate (Aldrich) in a mixture solvent of 40 mL ethanol, 40 mL DI water, and 80 mL hexane. The solution was heated to 70 ℃ in a water bath and kept at the temperature for 4 hours. Then, the upper organic layer was washed 3 times with 100 mL distilled water in a separatory funnel. The organic phase is then collected and dried in vacuum oven at 60 ℃ overnight.

Next, the Fe_3O_4 nanoparticles were synthesized from the iron-oleate complex as described above. 3.6 g of the iron-oleate complex was dissolved in a mixture solvent of 1 mL oleic acid (Aldrich) and 20 mL 1-octadecene (Acros Organics). The mixture was heated up to 320 ℃ in N_2 atmosphere, and kept at the temperature for 30 min. The resulting solution containing the nanocrystals was then cooled to room temperature. The resulting Fe_3O_4 nanoparticles have a diameter of 10.7±0.7 nm (Supplementary Figure 1a, b).

After the synthesis, the Fe_3O_4 nanoparticles were thoroughly washed, dried, and redispersed in hexane with known mass concentration. Typically, 2 mL crude reaction solution was mixed with 2 mL chloroform, 1 mL acetone, and 4 mL ethanol, sonicated, and centrifuged three times (Eppendorf Centrifuge 5804, 7500 rpm, 5 min). After the first and second centrifugation, the remaining sediment was dispersed with 1.2 mL hexane and 1.5 mL of ethanol. We kept ~100 μL sediments after each centrifugation unless otherwise stated. After the third centrifugation, the remaining sediment transferred to a petri dish with 0.5 mL hexane, and it was dried in vacuum oven at room temperature overnight. Then, the Fe_3O_4 nanoparticles suspension in hexane (0.3 mg/mL) were prepared for the interfacial self-assembly experiment.

Supplementary Note 2

A cylindrical glass container with ~3 cm diameter and ~2 cm depth was used for the interfacial self-assembly experiment. 2 mL diethylene glycol (DEG, Thermo Fisher) was added to the container as the lower liquid layer. Then, 80 μL hexane and 80 μL Fe_3O_4 nanoparticles suspension in hexane (0.3 mg/mL, described in Supplementary Note 1) were added on top of the DEG layer, and the container was quickly covered with glass slide to avoid fast evaporation of hexane. The Fe_3O_4 SL was obtained at the DEG-air interface with the solution untouched for 3 days.

About 30 min before scooping the SL with the substrate (silicon wafer or graphene/Si/SiO_2), 2 mL acetonitrile (Alfa Aesar) was carefully added to the solution with a glass pipette, to lift the SL up and avoid scooping the less volatile DEG (Supplementary Figure 1c). Note that the tip of glass pipette should be immersed in the DEG layer. Then, the plasma cleaned silicon wafers, or silicon wafers with graphene layer

were used to scoop the SL from the acetonitrile-air interface. The single layer region on silicon wafers can extend over tens of μm with good hexagonal order (Supplementary Figure 1d, e). We also annealed the obtained Fe_3O_4 SL on silicon wafer in forming gas (100 sccm H_2, 1000 sccm N_2) at 300 °C for 30 min, to remove excess ligand and enhance the electrical contact between Fe_3O_4 and graphene. There was no obvious change to the packing structure of Fe_3O_4 nanoparticles after annealing (Supplementary Figure 1f).

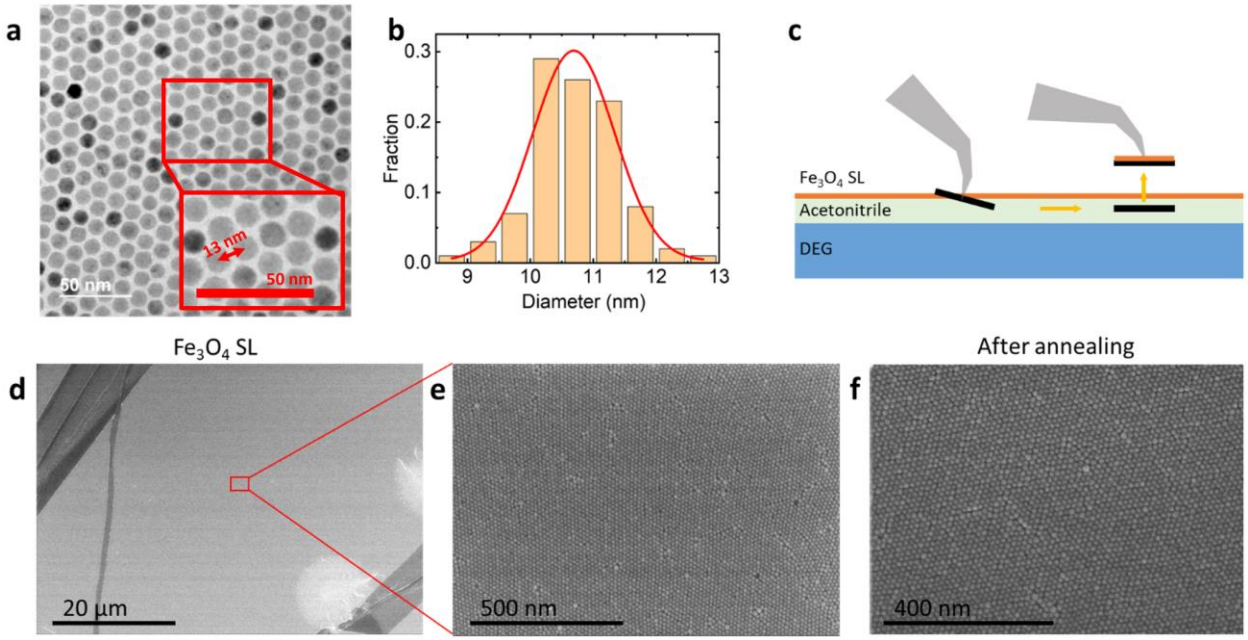

Supplementary Figure 1. Fe_3O_4 nanoparticles and SL. (a) TEM image of Fe_3O_4 nanoparticles. (b) Histogram of diameter of Fe_3O_4 nanoparticles measured from (a). (c) Schematic of Fe_3O_4 SL scoop up process. (d,e) Low and high magnification SEM image of Fe_3O_4 SL on silicon wafer. (f) High magnification SEM image of Fe_3O_4 SL after annealing.

The TEM image (Supplementary Figure 1a) and the SEM image (Supplementary Figure 1f) show the NSs with the hcp structure. Both images show some NSs with different colors. The variations in brightness or darkness among the NSs can be attributed to several factors, such as crystallinity, defects and height variations, crystallographic orientation, and variations in chemical composition. It is experimentally quite challenging to determine the chemical composition and the magnetic properties, which can be strongly dependent of chemical composition, of individual NSs. If some of the NSs (say the black/ darker ones in the TEM image) were not magnetic, they would behave as impurities in our superlattice system, which would just affect the strength of the resistivity steps in our transport data but not their positions.

Supplementary Figure 2 shows optical microscope images depicting deposition process of Fe_3O_4 SL on the graphene device in Hall bar configuration and confirming that the NSs form a monolayer atop graphene. a) state of the graphene device after opening a Poly (methyl methacrylate) (PMMA) window for NS deposition: The region in purple corresponds to graphene, the dark pink area represents the SiO_2 substrate, the light pink area indicates PMMA, and the light-yellow color corresponds to Au contacts. b) After depositing NS: The NS on the SiO_2 substrate looks in a different color (dark blue) than that of the NSs on graphene (light blue). c) After removing the PPMA from the entire device. d) After annealing to remove the organic ligand shell separating the NSs: the region in lightest blue corresponds to multilayer NS assemblies indicating the fact that the NS assemblies on the graphene Hall bar is monolayer, which is supported by the SEM images shown in Supplementary Figure 3.

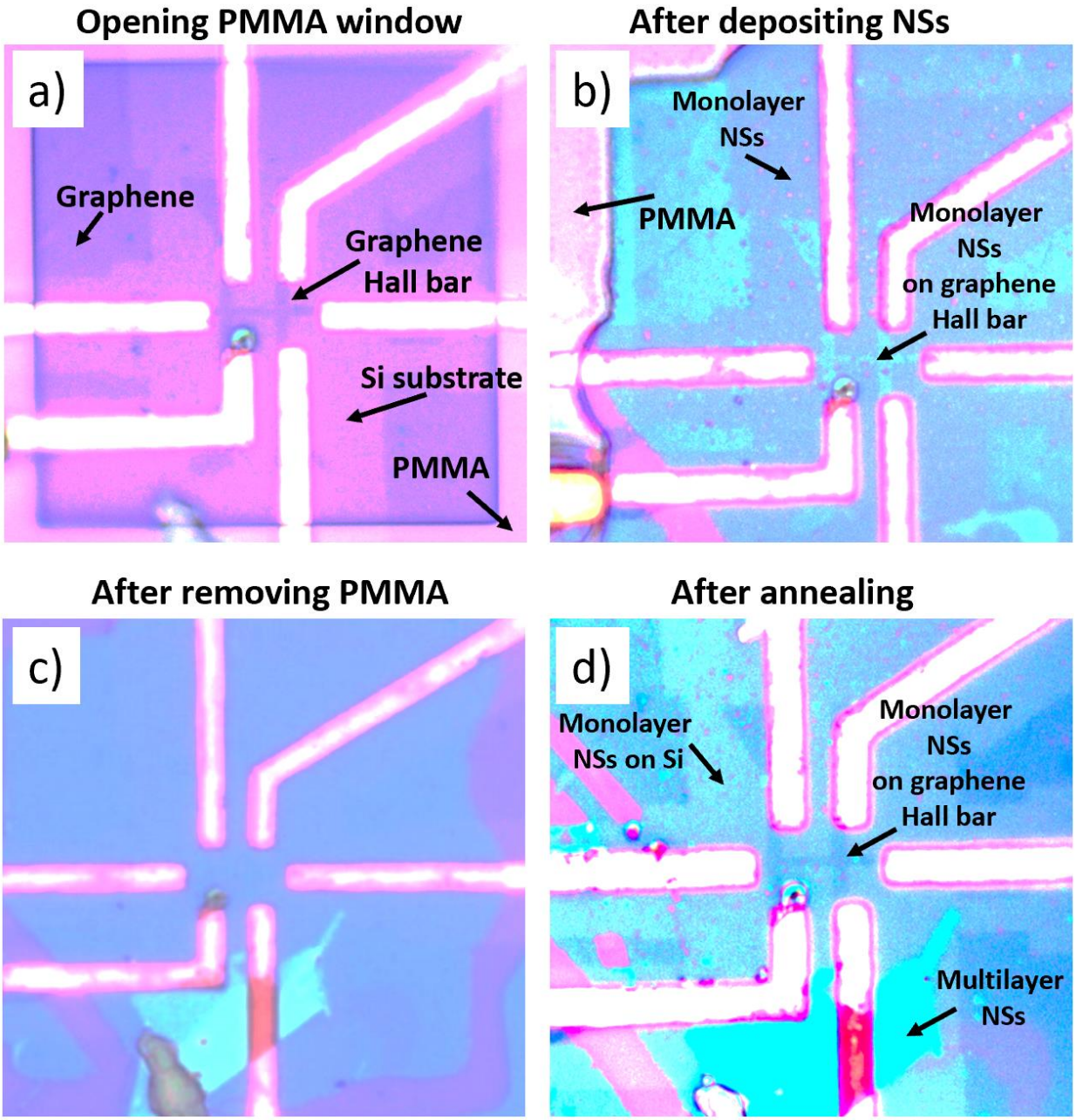

Supplementary Figure 2. Optical microscope images depicting the deposition of Fe_3O_4 nanosphere (NS) self-assemblies on the graphene device in Hall bar configuration and the state of the complete device after annealing. a) Opening a PMMA window for NS deposition. b) After depositing NSs c) After removing the PPMA from the entire device. d) After annealing to remove the organic ligand shell separating the NSs.

Supplementary Figure 3shows the SEM images of the graphene-NSs device measured consisting of regions with NSs on SiO_2 substrate only and graphene only, demonstrating that overall, the NSs maintain the same hcp structure as they have on the substrate. The hcp structure is evident both on the substrate and graphene, as can be seen from inset 1 and inset 2 of Supplementary Figure 3. The red dots in the inset 1 point out the hcp structure.

The NSs can diffuse much faster on the graphene than SiO_2 substrate due to graphene having no dangling bonds, and thus, the integrity of the NSs thin film may not be maintained across the device with micron size dimensions. As can be seen from the SEM images in Supplementary Figure 3, some sections of the monolayer NSs thin film peeled off the graphene (see inset 1). This should not influence the position of the superlattice Dirac points, although it may weaken the superlattice Dirac points due to the disorder. Our earlier work shows how disorder weakens but does not destroy the superlattice Dirac points [2].

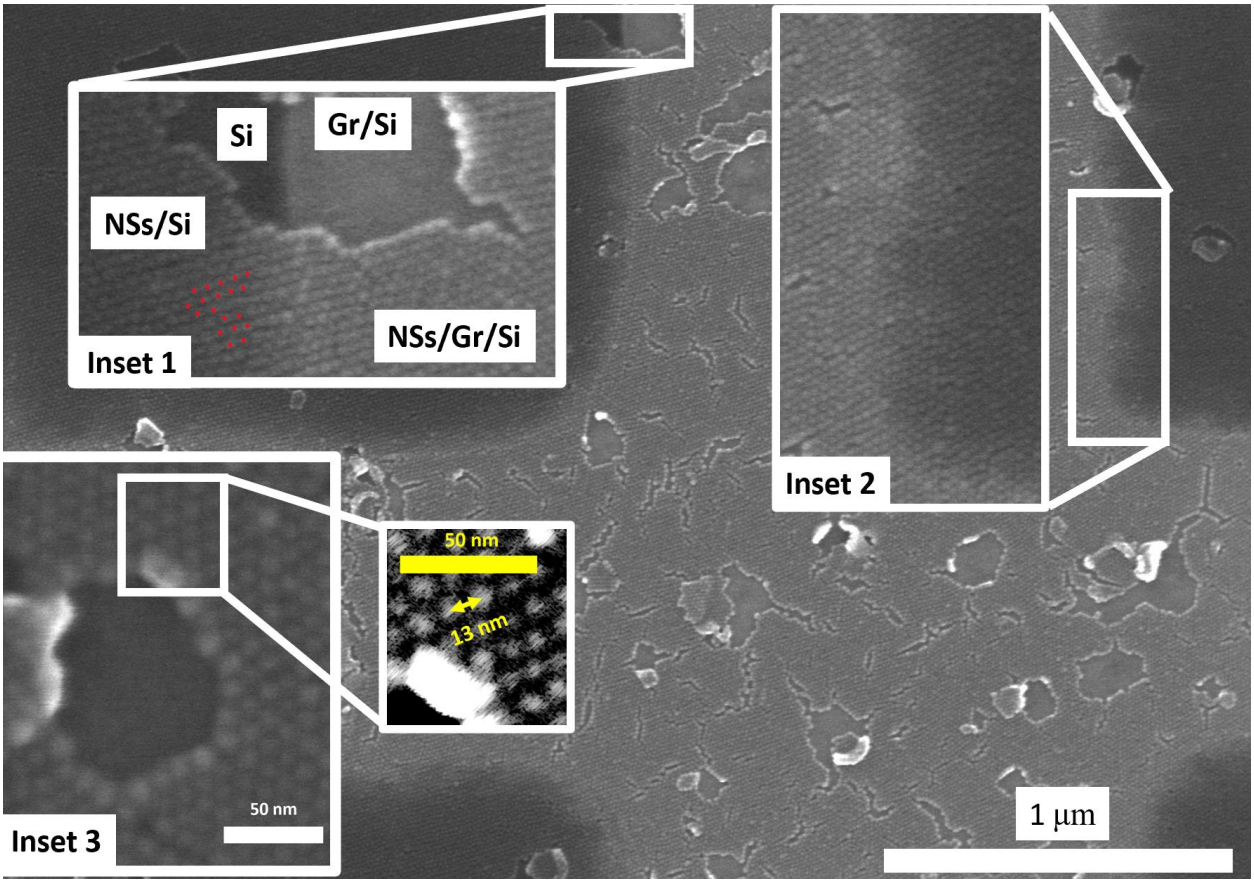

Supplementary Figure 3. An SEM image showing a portion of the graphene magnetic superlattice device measured. The scale bar: 1 μm. Inset 1 shows the hcp structure of the monolayer nanosphere assemblies (indicated by red dots), nanospheres on SiO_2 (darker regions where the nanospheres reside), and nanospheres on graphene which is on SiO_2. (lighter regions where the nanospheres reside). Inset 2 shows a clear/ sharp contrast between the region with graphene and without graphene. Inset 3 displays a region where the monolayer nanosphere film peeled off with no periodic color contrast pointing to possible physical holes left beneath the Fe_3O_4. Inset 3 also displays that the NSs are separated by 13 nm (False color used to show the average distance between the NSs). The scale bar: 50 nm.

From inset 1 of Supplementary Figure 3, one can see a region where the NSs peeled off along an edge between the SiO_2 substrate and the graphene. In the image, the graphene that had been under the NS is clearly intact, with a straight edge differentiating graphene (lighter color) from the SiO_2 substrate (darker color). This provides evidence that the graphene Hall bar underneath the NSs did not get damaged during the annealing process. Moreover, inset 3 shows clearly that graphene (after the monolayer NSs film peeled off) has no periodic color contrast meaning that there is no periodic spacing of physical holes left behind beneath the Fe_3O_4.

Possible dust on the SiO_2 substrate, residues of PMMA after electron-beam lithography, and residues of ligands covering the NSs can result in height variations and variations in the wettability of graphene, which can give rise to disorder in the monolayer NS thin films and affect only the integrity of the film (some parts of NS assembly peeled off) but does not affect the hcp structure drastically or modify the superlattice effects observed in transport.

Supplementary Note 3

Monolayer graphene, grown on 35um thick copper foil using chemical vapor deposition, purchased from ACS Material LLC, was transferred onto SiO_2(300 nm)/Si substrates using standard wet transfer techniques. A 0.1 M aqueous solution of ammonium persulfate was used to etch the copper layer away. The graphene layer, supported by a ~200 nm thick layer of PMMA, was then scooped onto the substrate. After the sample was dried, the PMMA layer was removed by acetone.

The transferred graphene was then etched into a Hall bar geometry using electron beam lithography, with 950 PMMA A4 (purchased from Kayaku Advanced Materials) acting as a positive resist, and oxygen plasma reactive ion etching. The Hall bar device described in this manuscript is of length $L = 6$ μm and width $W = 1$ μm. A second e-beam lithography step, along with e-beam metal evaporation, was used to pattern Ti (5 nm)/Au (20 nm) electrodes onto the graphene Hall bar.

A third e-beam lithography step was used to create a 'window' in the PMMA-resist layer, selectively at the location of the graphene device. After the iron oxide (Fe_3O_4) nanospheres (NS) were transferred onto the sample, this layer of PMMA was removed via acetone. Thus, the self-assembly of iron oxide NS covered only the graphene Hall bar device and not the entirety of the chip. Thermal annealing under forming gas at 300 C for 30 min was performed to remove the organic ligand shell around the NS on the graphene Hall bar device.

The device was wire-bonded, and all transport measurements were performed inside a Quantum Design Physical Property Measurement System (Quantum Design PPMS Dynacool) which uses pulse tube refrigeration to cool down to a base temperature of 1.8 K and is equipped with a 9 T superconducting magnet in the out-of-plane direction. Measurements were performed via the lock-in technique in an AC current bias mode (100 nA, 14 Hz) using National Instruments SR830 lock-in amplifiers. The gate voltage was tuned using a Tektronix Keithley 2400 Source meter.

The magnetic properties of the nanoparticles were characterized using SQUID magnetometry in a Quantum Design Magnetic Property Measurement System (MPMS3) with a standard quartz holder for in-plane magnetization measurements and a straw holder for out-of-plane measurements.

Supplementary Note 4

We took the second derivative of the resistivity as a function of gate voltage data in order to remove the background Dirac peak to obtain the low frequency of the resistance peaks in Supplementary Figure 4a below. Here, we validate the frequency of the zero-field resistance dips, which are labeled and presented in Supplementary Figure 4b in a systematic way by the FFT analyses. We smoothed the second derivative by creating B-spline of the data in order to have more data points for a proper FFT analysis. It can be seen from the Supplementary Figure 4c that the second derivative and its B-spline overlap which would create no difference in our FFT analysis. Supplementary Figure 4d shows the FFT of the second derivative. The prominent peak is 1.4 V, and it is consistent with the determined dip positions in Supplementary Figure 4a and Supplementary Figure 4b.

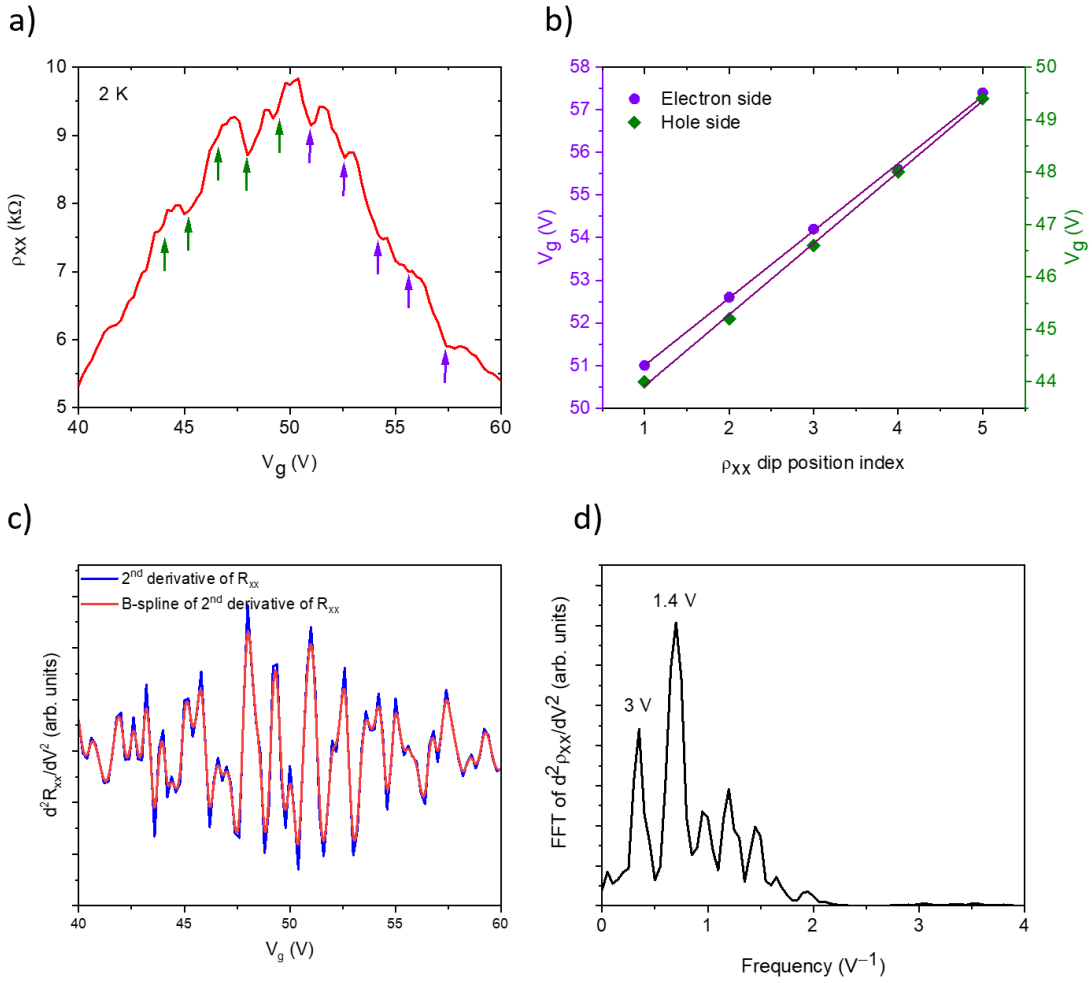

Supplementary Figure 4. Quasiperiodic resistivity oscillations in magnetic superlattice of graphene: a) Gate voltage dependence of ρ_{xx} at 2 K between 40 and 60 V. Nearly equally spaced resistivity peaks are indicated by green arrows for the hole side and the purple arrows for the electron side. The resistivity dips for both the hole and electron sides occur in nearly equal spaced gate voltage values as shown in (b) and the spacing was determined to be 1.4 V by the second derivative of the resistivity (c) and the fast Fourier transform analyses as shown in (d).

Supplementary Note 5

The value of M_{NS} has been selected by starting with the experimental device geometry and then subsequently solving for the self-consistent ground state energies (here defined as consistency between the quantum transport and the electrostatics) assuming that the charge neutrality point is located at Vg = 50 V. The value of the peak magnetization on the nanospheres is varied until the relative peak spacing in measured resistivity are commensurate with that of the simulations in the zero external magnetic field case. From the simulations, the magnitude of the imparted magnetism that produces the proper spacing is as quoted in the main text.

In the simulations, the device geometry is entered for both graphene and the surrounding structure and then charge self-consistency is enforced until the energetic separation between the sucessive iterations is less than 10 μeV. As the structure simulated contains 300 nm thick SiO_2 layer, then the relative capacitance and field penetration is accounted for within the simulation construct with the assumption that we begin with the Dirac point located at Vg = 50 V. The successive changes in Vg, thus produce the changes in the chemical potential of graphene that we report in the text. On the other hand, we may obtain a relative check on the expected changes by using the capacitance of the structure.

We calculate the resistivity using two different methodologies. In the first, and more rigorous methodology, we apply the mechanics of the non-equilibrium Green's function formalism to calculate the current flowing within the graphene, as has been done in both our own work and in many other works. As a check, we calculated the inverse of the DoS and use the fact that, within linear response theory, the DoS at the Fermi level is proportional to the conductivity, roughly speaking. As both the careful and the crude calculations are in qualatative agreement then their use is interchangable. Therefore, in the manuscript, we have presented the inverse of the DoS as calculated at the various chemical potentials plotted.

We observe peaks in the DoS that have similar spacings and energy scales as the experimental peaks. While there is coincidence with the peaks between the experimental data and the theoretical calculations, the overall shape of the DoS in the calculations is quite different. The discrepancy between the shape of the DoS curves is attributed to the assumed quasiparticle lifetime in the calculations. Here we assume a quasiparticle lifetime, which enters the calculations via the Green's function [3], to be $\eta = 50\ \mu eV$. The selected lifetime produces sharper peaks in the DoS when compared to the experimental measurements, however, the broadening associated with the various levels of the graphene layer are also sharper leading to the need for a more refined mesh to be able to capture the contributions. In this manner, the discrepancy is directly attributed to a numerical discrepancy and not a physical inaccuracy.

Supplementary Note 6

The phase coherence length gives an approximation of how many superlattice periods the electrons remain coherent. Weak localization (WL) measurement provides information about the phase coherence length. The dephasing time, inter valley scattering, and intra valley scattering, which are forms of inelastic scattering, introduce corrections to the Drude resistivity. The quantum correction to magnetoresistance is determined by:

$$\Delta\rho_{xx}(B) = -\frac{e^2\rho_{xx}^2}{\pi h}\left[F\left(\frac{B}{B_\phi}\right) - F\left(\frac{B}{B_\phi + 2B_i}\right) - 2F\left(\frac{B}{B_\phi + B_*}\right)\right] \quad (1)$$

$$F(z) = \ln z + \Psi\left(\frac{1}{2} + \frac{1}{z}\right) \text{ and } B_{\phi,i,*} = \frac{h}{8\pi De}\tau_{\phi,i,*}^{-1}$$

where B is the magnetic field, Ψ is the digamma function, $D = v_F l_\mu/2$ is the diffusion constant, v_F = 10^6 m/s is the Fermi velocity, l_μ is the mean free path of the Drude model, τ_ϕ,i,* are the dephasing, inter-valley, and intravalley scattering times [4]. The experiment involves sweeping the magnetic field range from -0.6

T to 0.6 T while measuring the resistance at a temperature of 2 K. These measurements are then utilized to determine dephasing time by fitting the data using equation (1). The fitting process yields a phase coherence length (L_ϕ) of approximately 91 nm for $V_g = 0$ V and 112 nm $V_g = -20$ V by using $L_\phi = \sqrt{D\tau_\phi}$.

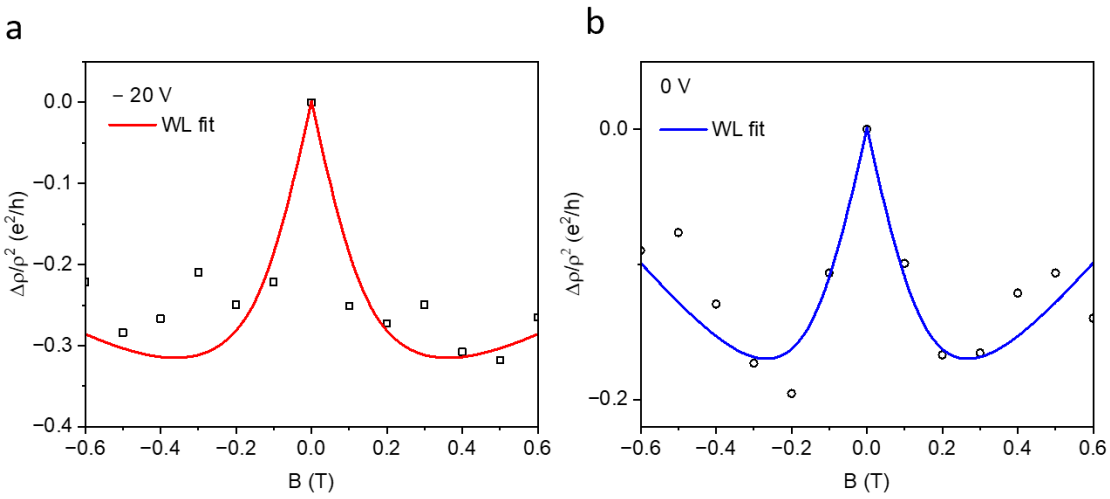

Supplementary Figure 5. Fitting magnetoresistance at – 20 and 0 V to weak localization (WL) theory. (a) $V_g = -20$ V, (b) $V_g = 0$ V.

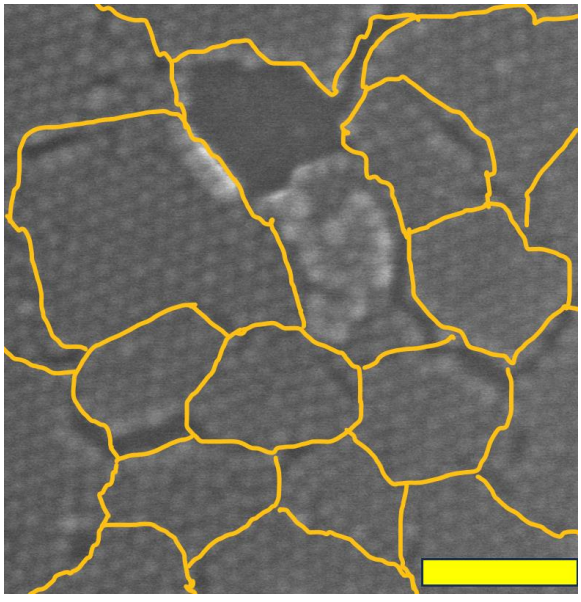

Supplementary Figure 6. SEM image of a monolayer NS assembly with each region enclosed by orange lines depicting a single-crystalline domain. Scale bar: 100 nm.

Supplementary Note 7

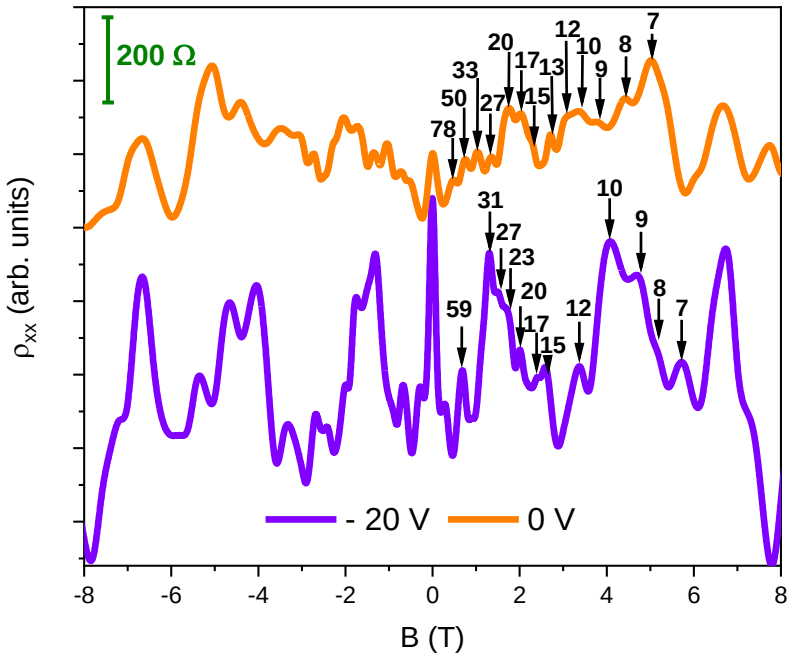

Supplementary Figure 7. Commensurate magnetoresistance peaks in graphene magnetic nanospheres superlattice system.

All the MR peaks are pointed with arrows showing the number of nanospheres or hole-like regions enclosed by cyclotron orbits.

Supplementary References

1. Park, J.; An, K.; Hwang, Y.; Park, J.G.; Noh, H.J.; Kim, J.Y.; Park, J.H.; Hwang, N.M.; Hyeon, T., Ultra-large-scale syntheses of monodisperse nanocrystals. *Nature materials* **2004**, *3* (12), 891-895.
2. Zhang, Y.; Kim, Y.; Gilbert, M. J.; Mason, N., Electronic transport in a two-dimensional superlattice engineered via self-assembled nanostructures. *npj 2D Materials and Applications* **2018**, *2* (1), 1-6.
3. Akis, R.; Ferry, D.K.; Gilbert, M.J; Goodnick, S.M., Quantum Transport at Nanoscale. In *Handbook of Nanoscience, Engineering, and Technology* CRC Press **2018** (68-89).
4. Morpurgo, A. F.; Guinea, F., Intervalley scattering, long-range disorder, and effective time-reversal symmetry breaking in graphene. *Physical review letters* **2006**, *97* (19), 196804.